
Supporting Information

A Columnar Liquid Crystal with Permanent Polar Order

J. Guilleme,^a J. Aragón,^b E. Ortí,^b E. Cavero,^c T. Sierra,^{c,*} J. Ortega,^d C. L. Folcia,^e J. Etxebarria,^{e,*} D. González-Rodríguez^{a,*} and Tomás Torres^{a,*}

^a Departamento de Química Orgánica, Universidad Autónoma de Madrid, 28049 Madrid, Spain.

^b Instituto de Ciencia Molecular, Universidad de Valencia, 46980 Paterna (Valencia), Spain.

^c Departamento de Química Orgánica, Facultad de Ciencias – Instituto de Ciencia de Materiales de Aragón (ICMA), CSIC – Universidad de Zaragoza, 50009 Zaragoza, Spain.

^d Departamento de Física Aplicada II; Facultad de Ciencia y Tecnología, UPV/EHU, 48080, Bilbao, Spain.

^e Departamento de Física de la Materia Condensada, Facultad de Ciencia y Tecnología, UPV/EHU, 48080, Bilbao, Spain.

Supporting Information Available:

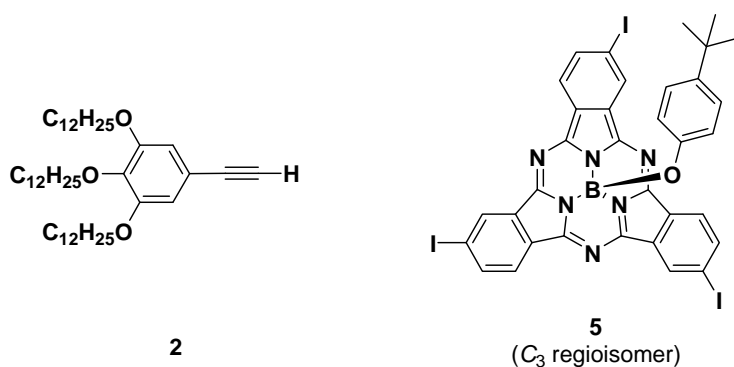
Synthesis and Molecular Characterization	S2
• General Methods and Synthetic Schemes	S2
• Synthetic procedures and characterization data	S3
Liquid Crystal Characterization	S10
• Thermal characterization and liquid crystalline behavior	S10
• AFM measurements	S11
• X-ray diffraction studies	S14
SHG Measurements	S16
Theoretical Calculations	S18
References	S22

SYNTHESIS AND MOLECULAR CHARACTERIZATION

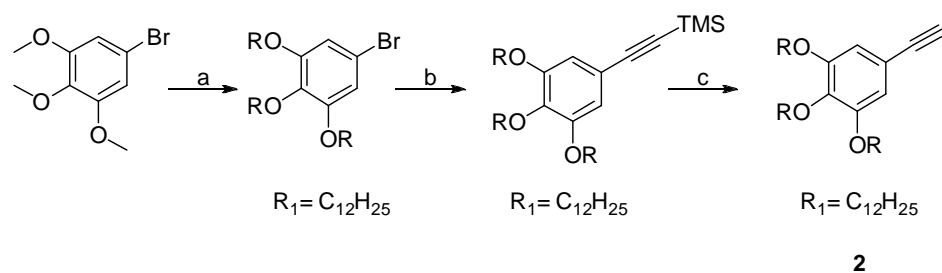
General Methods.

Synthesis and Characterization. UV/Vis spectra were recorded with a JASCO V-660. MALDI-TOF-MS spectra were obtained from a BRUKER ULTRAFLEX III instrument equipped with a nitrogen laser operating at 337 nm. NMR spectra were recorded with a BRUKER AC-300 (300 MHz) instrument. The temperature was actively controlled at 298 K. Chemical shifts are measured in ppm relative to the correspondent deuterated solvent. Carbon chemical shifts are measured downfield from TMS using the resonance of the deuterated solvent as the internal standard. Column chromatography was carried out on silica gel Merck-60 (230-400 mesh, 60 Å), and TLC on aluminum sheets precoated with silica gel 60 F254 (E. Merck).

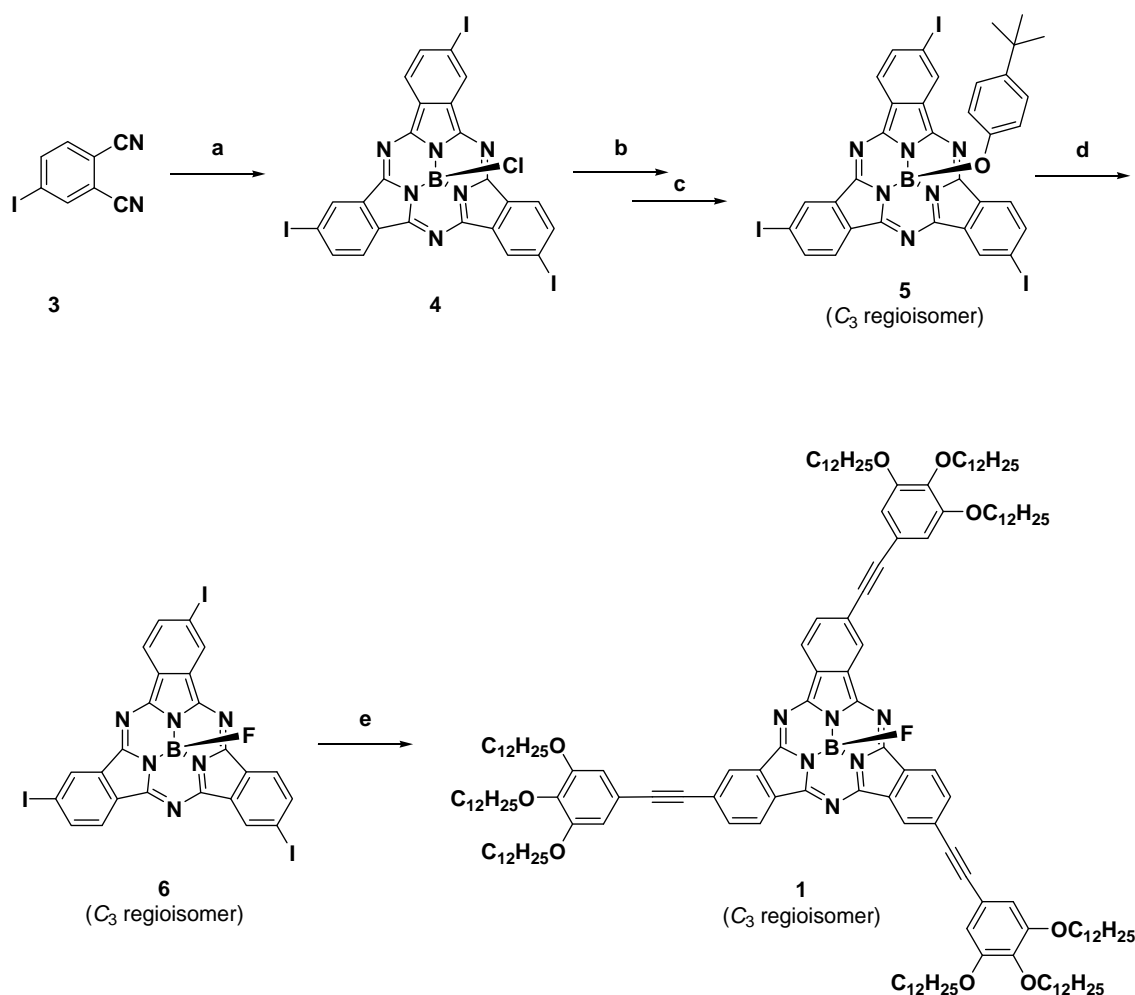
Starting Materials. Chemicals were purchased from commercial suppliers and used without further purification. Solid, hygroscopic reagents were dried in a vacuum oven before use. Reaction solvents were thoroughly dried before use using standard methods. The synthesis and characterization of the starting 3,4,5-tri(dodecyloxy)phenylacetyleneⁱ **2** and subphthalocyanine **C₃-5ⁱⁱ** have been previously reported.



Synthetic procedures and characterization data

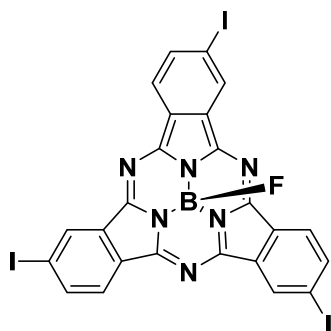


Scheme S1. Synthesis of 3,4,5-Tri(dodecyloxy) phenylacetylene (**2**). a) BBr₃; H₂₅C₁₂Br, K₂CO₃; b) trimethylsilylacetylene, Pd(PPh₃)₄, CuI, piperidine, 85°C; c) K₂CO₃, CH₂Cl₂/Methanol.



Scheme S2. Synthesis of compound **1**. a) BCl₃ (*p*-xylene), 180 °C; b) 4-(*tert*-butyl)phenol, toluene, reflux; c) C₃ and C₁ Regio-isomer separation by column chromatography; d) BF₃·(Et₂O), toluene; e) **2**, PdCl₂(PPh₃)₂, CuI, rt, THF.

SubPcBF 6



I₃-SubPc-F **6** was synthesized adapting the procedure of Timothy P. Bender et alⁱⁱⁱ. **5** (150 mg, 0.162 mmol) was placed in a 10 mL flask under argon atmosphere and dissolved in 1.5 mL of dry toluene. Boron trifluoride diethyl etherate (Et₂O·BF₃, 0.6 mL, 25 mol equiv.) was added dropwise and the color of the solution turned immediately blue. The solution was heated to reflux for 3 hours. At this point, pyridine was added dropwise until the solution turned pink again. The organic phase was washed with a solution of NaOH (0.05 M) and dried with Mg₂SO₄. After adding a few drops of methanol to the organic phase, the product precipitated and it was finally filtered. The resulting purple solid was dried in a vacuum oven overnight. Yield: 91%.

Mp > 250 °C.

¹H-NMR (300 MHz, THF-d₈): δ (ppm) = 9.22 (s, 3H), 8.60 (d, 3H), 8.30 (d, 3H).

¹⁹F-NMR (300 MHz, THF-d₈): δ (ppm) = -159.77.

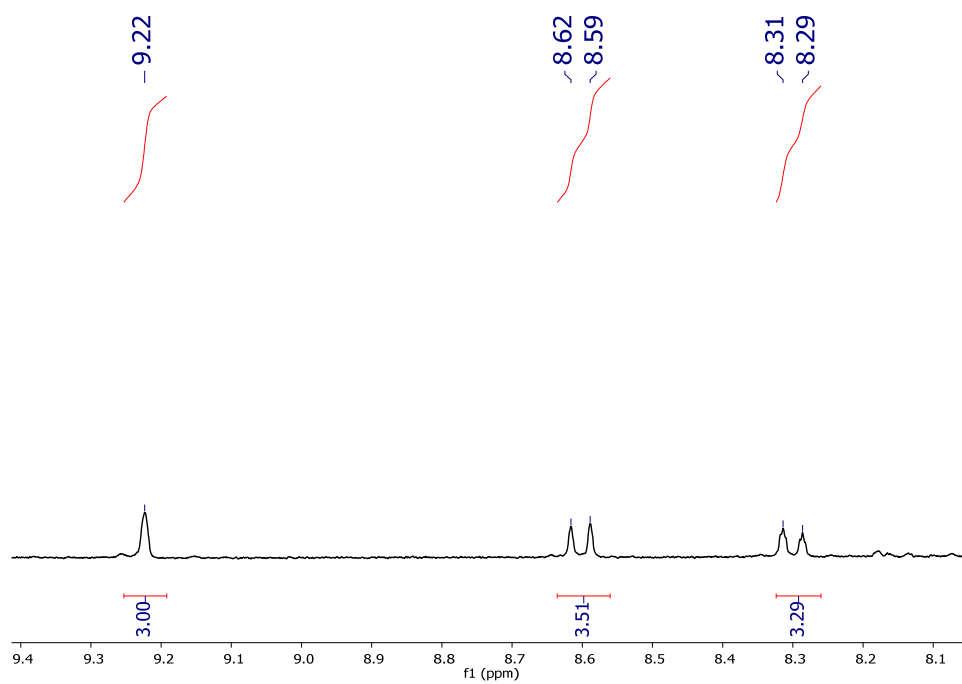
UV-vis (dioxane): λ_{\max} (nm) = 569, 549 (sh), 517, 333.

MS (MALDI-TOF, DCTB): m/z = 791.8 (100%).

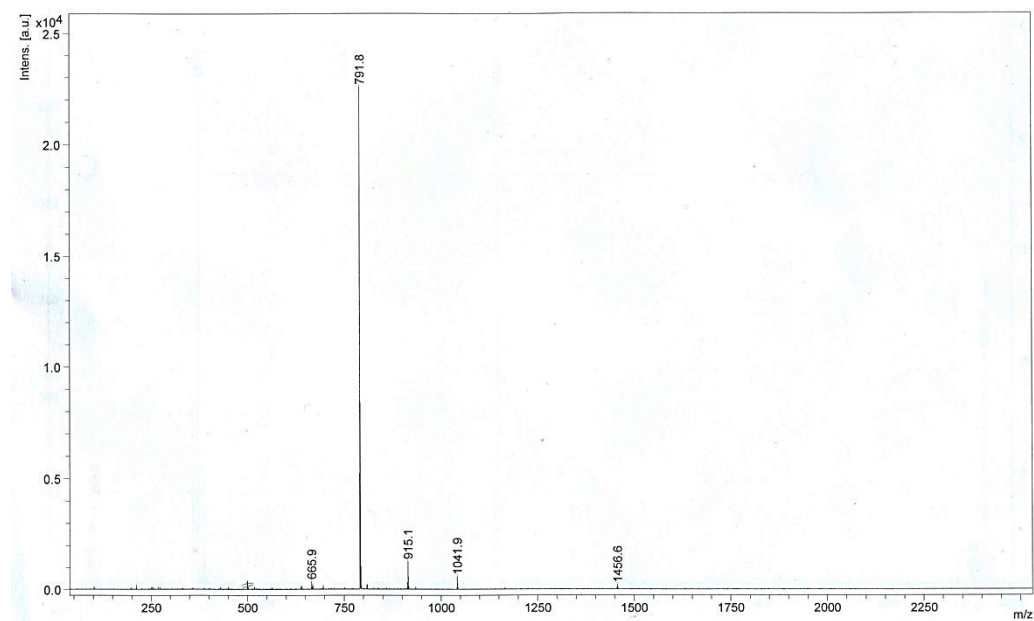
HRLSI-MS (C₂₄H₉BF₃N₆) [M]⁺: Calculated: 791.8100

Found: 791.8099

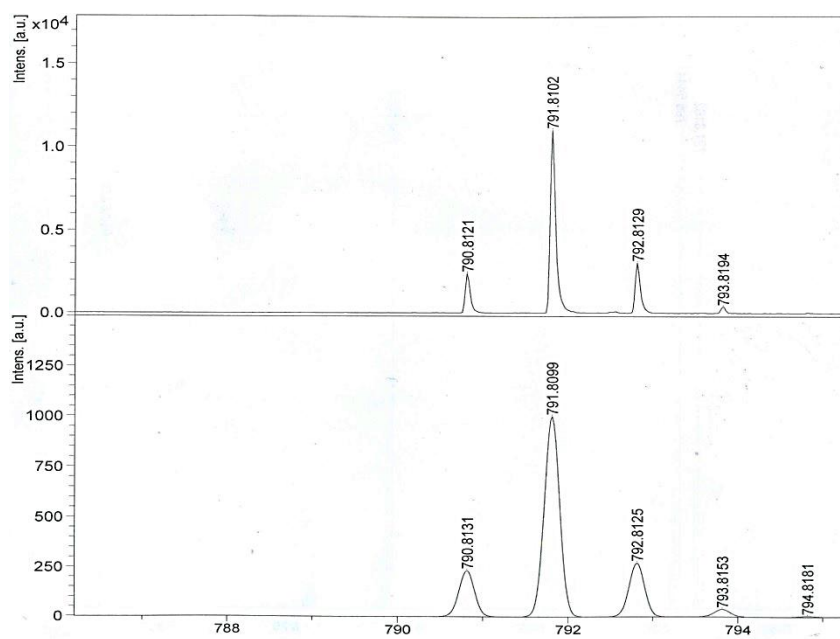
Due to its low solubility it was impossible to obtain a proper ¹³C-NMR spectrum.



$^1\text{H-NMR}$ (300 MHz, THF-d8) of **6**

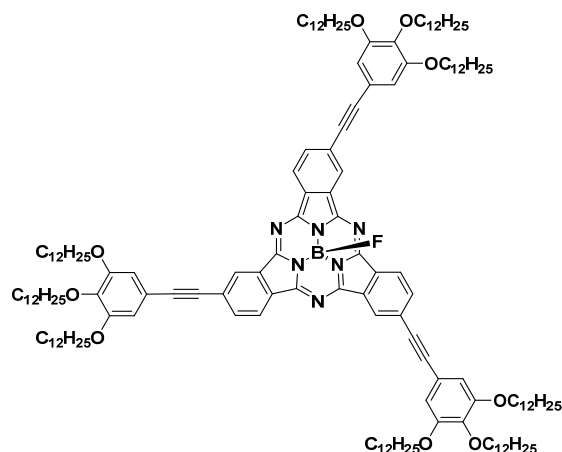


MS (MALDI-TOF, DCTB) of **6**



HRLSI-MS of **6**

SubPc 1



A mixture of 40 mg of C_3 triiodosubphthalocyanine **6** (0.05 mmol), 7 mg of $PdCl_2(PPh_3)$ (0.009 mmol) and 1.7 mg of CuI (0.009 mmol) were placed in a 25 mL two-neck flask. Subsequently, 3 mL of THF/ Et_3N (5:1) were added. The mixture was degassed by three “freeze-pump-thaw” cycles, 3,4,5-tri(dodecyloxy)phenylacetylene was added to the solution and was stirred at room temperature overnight. When the reaction was completed, it was filtered through celite and the solvent was evaporated under reduced pressure. The product was purified by column chromatography on silica gel using DCM/Hexane (3:1) as eluent. The resulting solid was washed with methanol to afford a purple solid in a 55% Yield.

1H -NMR (300 MHz, $CDCl_3$): δ (ppm) = 9.02 (s, 3H), 8.80 (d, 3H), 8.02 (d; 3H), 6.84 (s, 6H), 4.04 (m, 18H), 1.85 (m, 18H), 1.51 (m; 18 H), 1.39 (m, 144H), 1.36 (t, 27H).

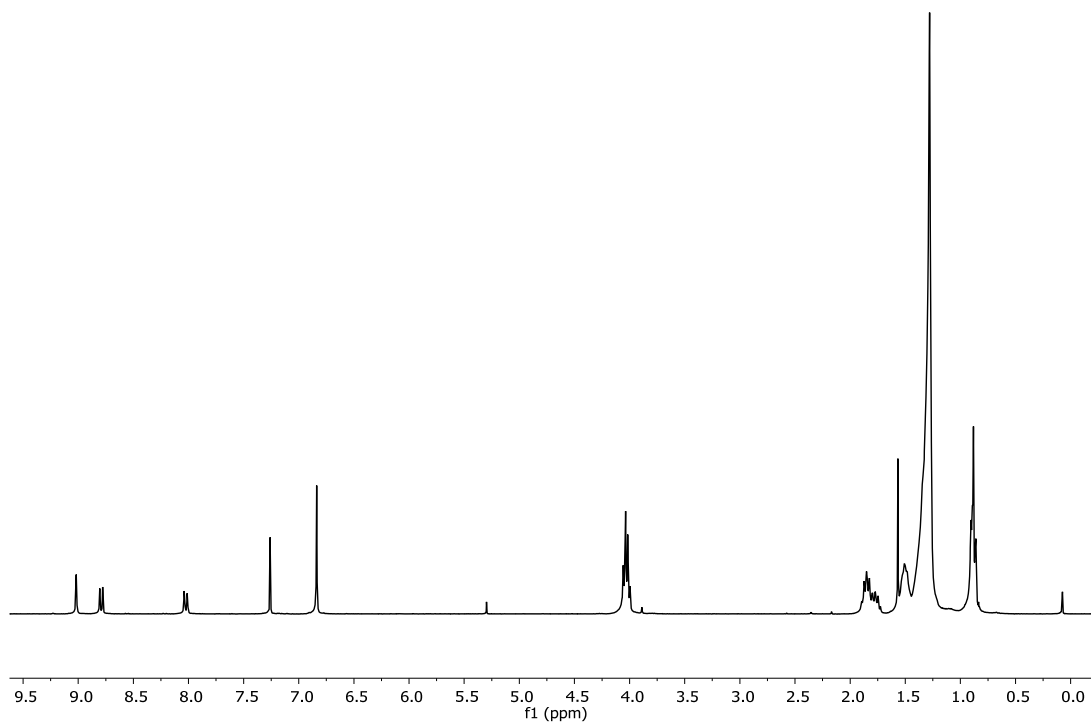
^{13}C -NMR (75.5 MHz, $CDCl_3$): δ (ppm) = 153.28, 151.30, 139.82, 132.96, 131.27, 129.84, 125.65, 122.36, 117.22, 114.94, 110.52, 93.23, 88.31, 73.76, 69.39, 32.09, 30.50, 29.90, 29.86, 29.81, 29.75, 29.57, 29.54, 29.52, 29.26, 22.84, 14.25.

MS (MALDI-TOF, DCTB): m/z = 2372.9 (100%)

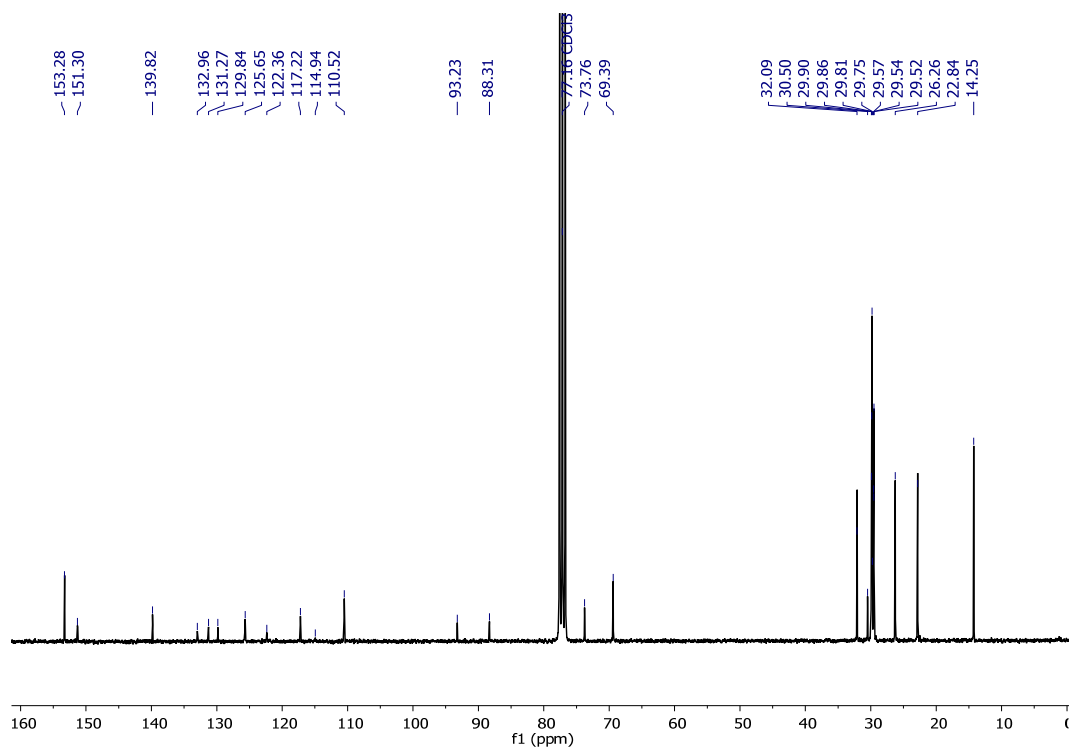
HRLSI-MS ($C_{156}H_{241}BFN_6O_9$) $[M+H]^+$: Calculated: 2372,8662

Found: 2372.8681.

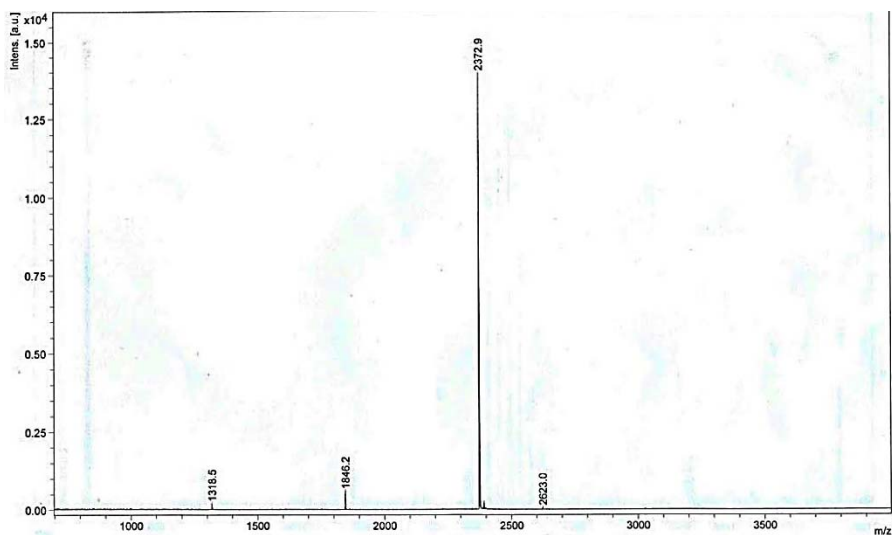
UV-vis (MCH): λ_{max} (nm) ($\log \epsilon$ ($dm^3 mol^{-1} cm^{-1}$)) = 587 (4.99), 566 (sh), 539 (4.45), 376 (4.53), 309 (4.49).



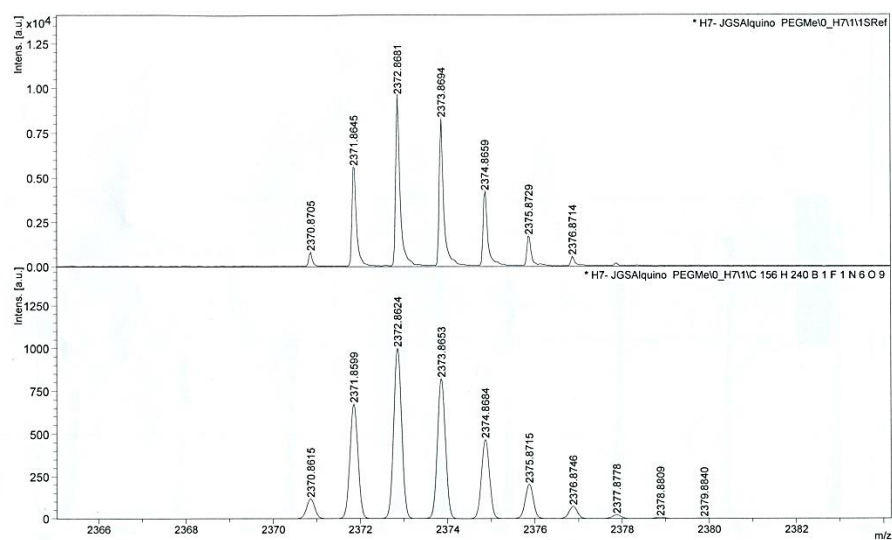
$^1\text{H-NMR}$ (300 MHz, CDCl_3) of **1**



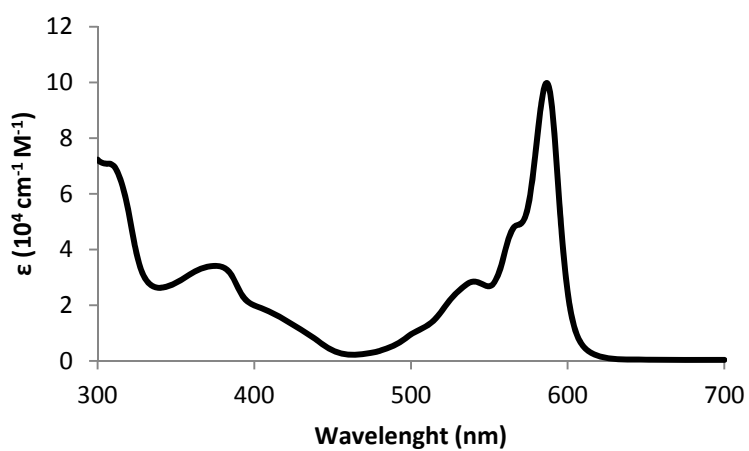
$^{13}\text{C-NMR}$ (75.5 MHz, CDCl_3) of **1**



MS (MALDI-TOF, DCTB) of **1**



HRLSI-MS of **1**



UV-vis in MCH ($3.2 \times 10^{-5} \text{ M}$) of **1**.

LIQUID CRYSTAL CHARACTERIZATION

Thermal characterization and liquid crystalline behavior

Thermogravimetric analysis (TGA) was performed using a TA Q5000IR instrument at a heating rate of $10\text{ }^{\circ}\text{C min}^{-1}$ under a nitrogen atmosphere. Thermal transitions were determined by differential scanning calorimetry (DSC) using a TA DSC Q-20 instrument under a nitrogen atmosphere with powdered sample (2.517 mg) sealed in aluminum pans. Liquid crystal textures were studied using an Olympus BX-50 polarizing microscope equipped with a Linkam TMS91 hot stage and a CS196 hot-stage central processor. Microphotographs were taken with an Olympus DP12-2 digital camera.

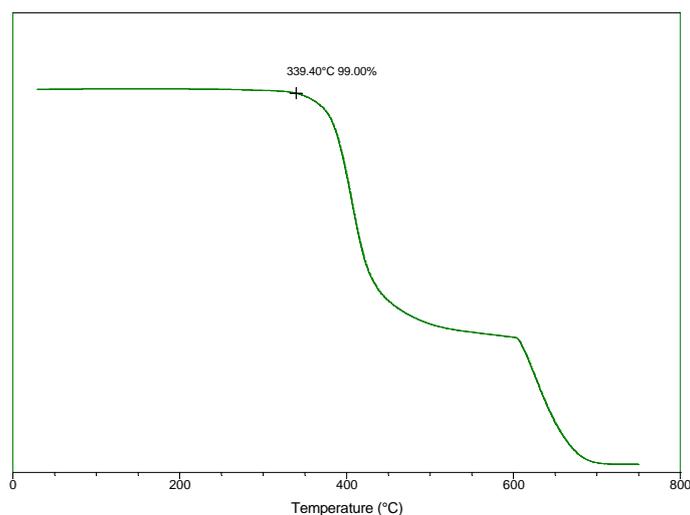


Figure S1. TGA thermogram recorded from room temperature to $750\text{ }^{\circ}\text{C}$, under N_2 atmosphere. A weight loss of 1% was calculated at $339.4\text{ }^{\circ}\text{C}$.

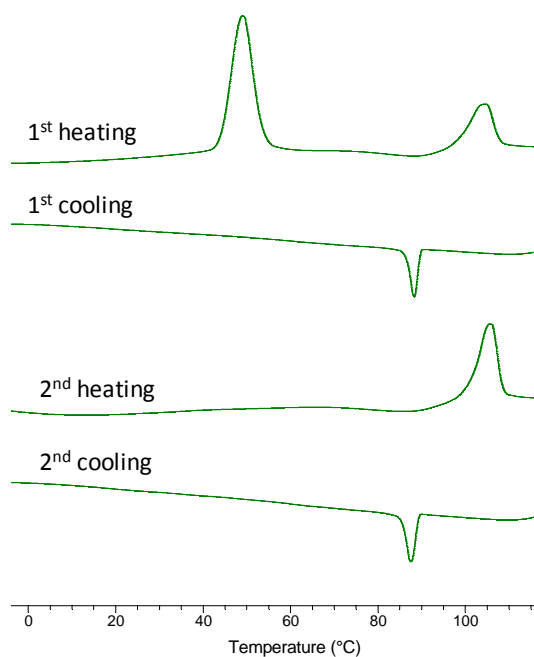
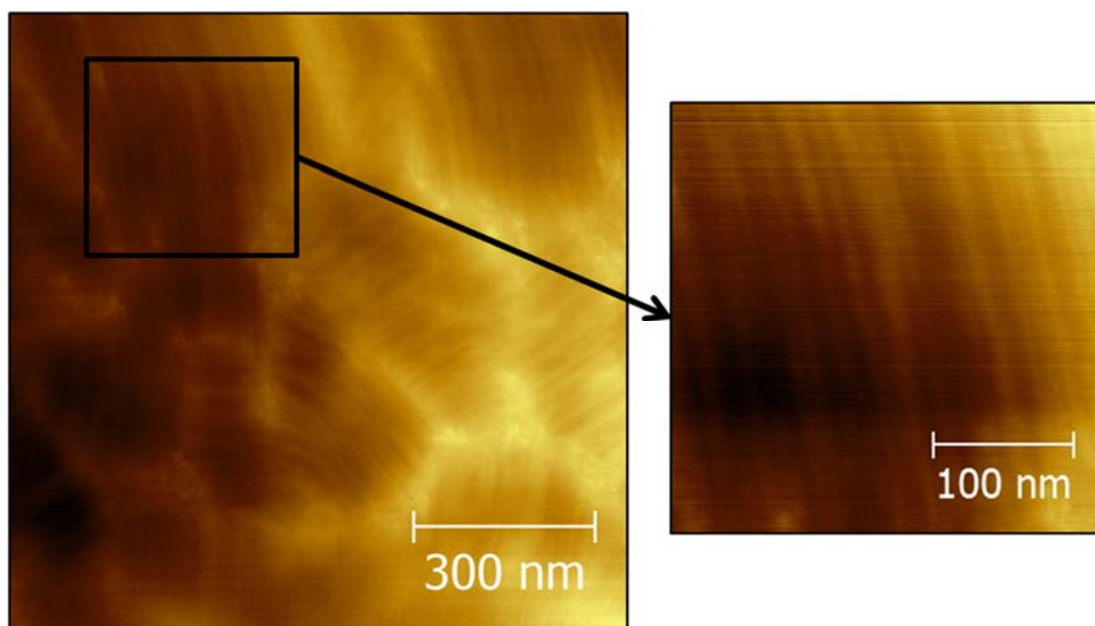


Figure S2. First and second heating-cooling cycle thermograms, recorded at a rate of $10\text{ }^{\circ}\text{C}/\text{min}$. Subsequent heating-cooling cycles reproduce the 2nd cycle.

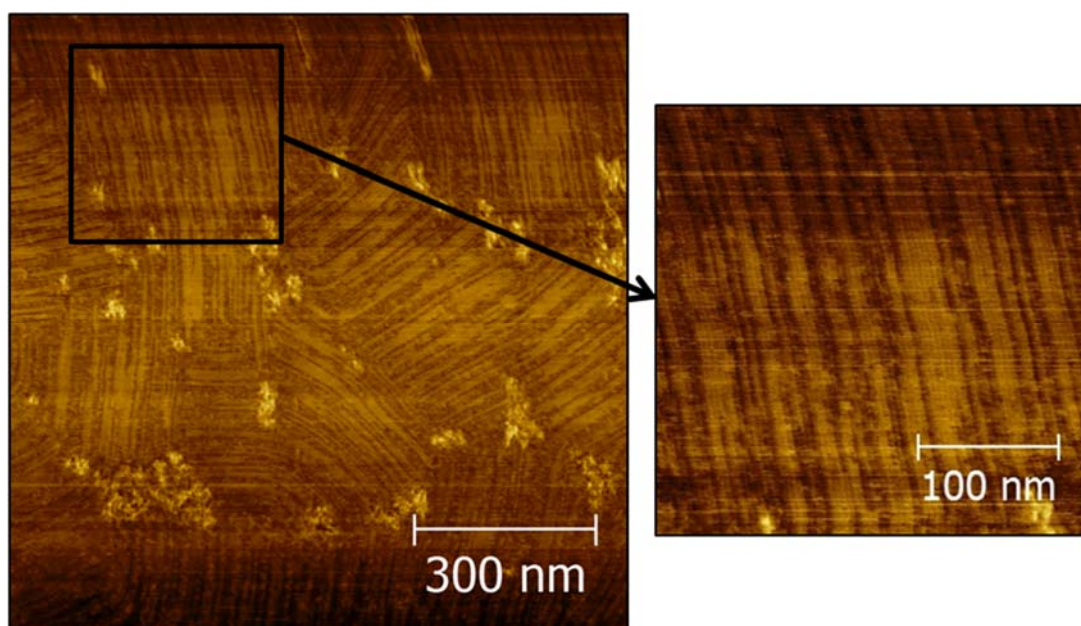
AFM studies

AFM measurements were performed on a Multimode 8 from Veeco-Bruker on tapping mode. Images were taken at room temperature for a thin sample of **1**, which was deposited on mica by casting a concentrated solution of **1** in dichloromethane and thermally treated by heating up to the isotropic liquid and cooling down at a rate of ca. 10 °C/min.

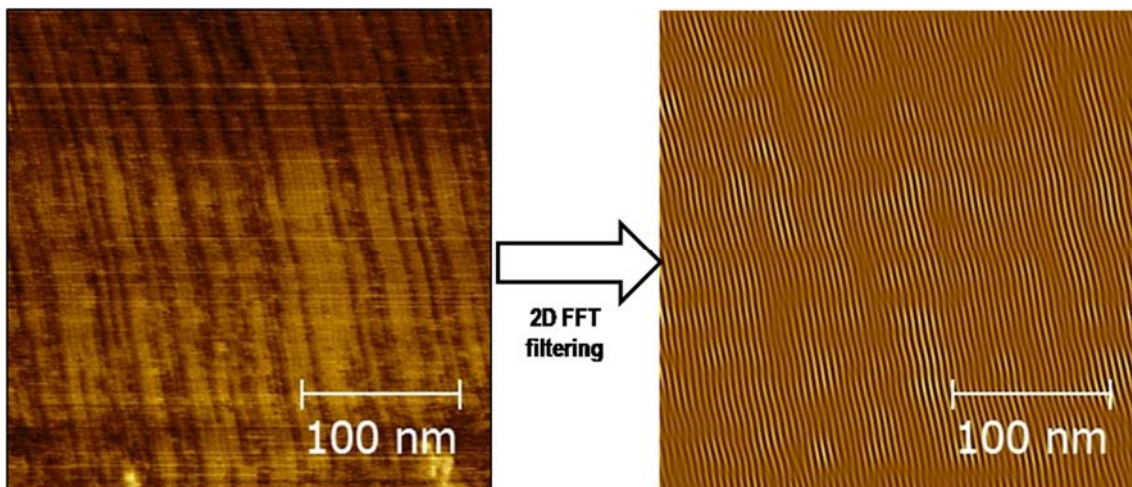
a)



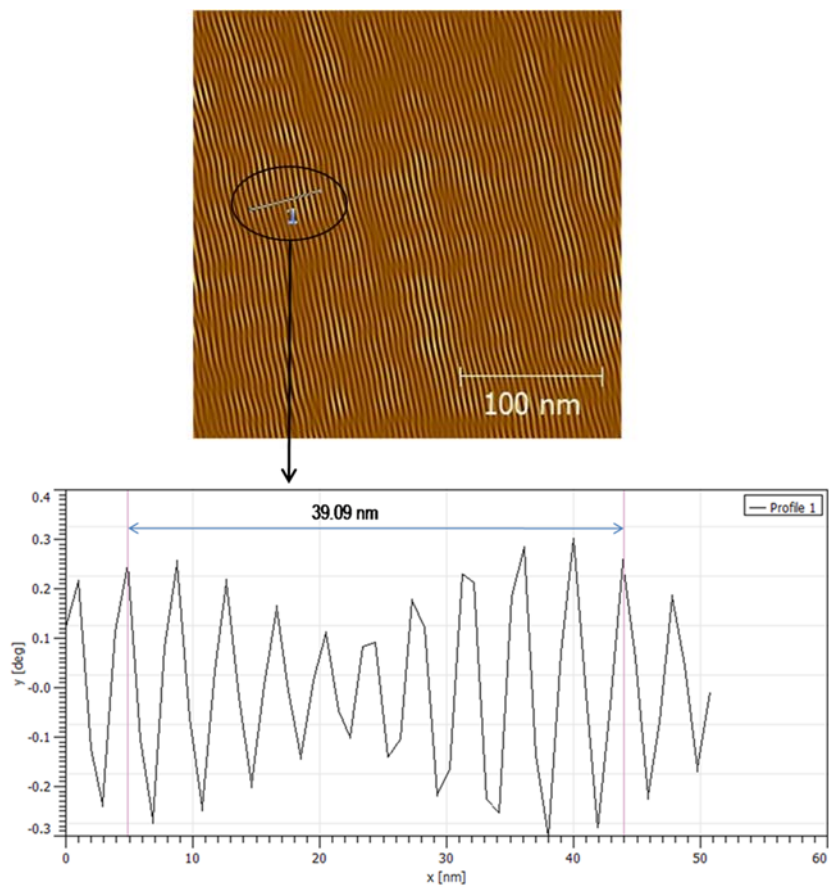
b)



c)



d)



e)

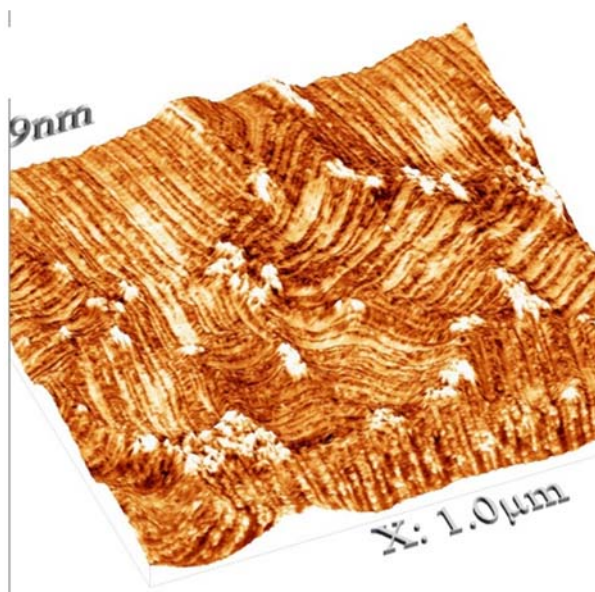


Figure S3: **a)** Topography images. **b)** Phase Images. **c)** Phase image and its 2D Fourier transform (2D FFT) filtering image. **d)** 2D FFT image and profile obtained to calculate an average distance between lines (ca. 3.9 nm). **e)** 3D phase image.

X-ray diffraction studies

The structure of the mesophase was determined by XRD measurements, which were carried out at room temperature using a Pinhole camera (Anton-Paar) operating with a point focused Ni-filtered Cu K α beam. The sample was held in Lindemann glass capillaries (0.6 and 1 mm diameter) perfectly sealed and heated, when necessary, with a variable-temperature attachment. The diffraction patterns were collected on a flat photographic film perpendicular to the X-ray beam.

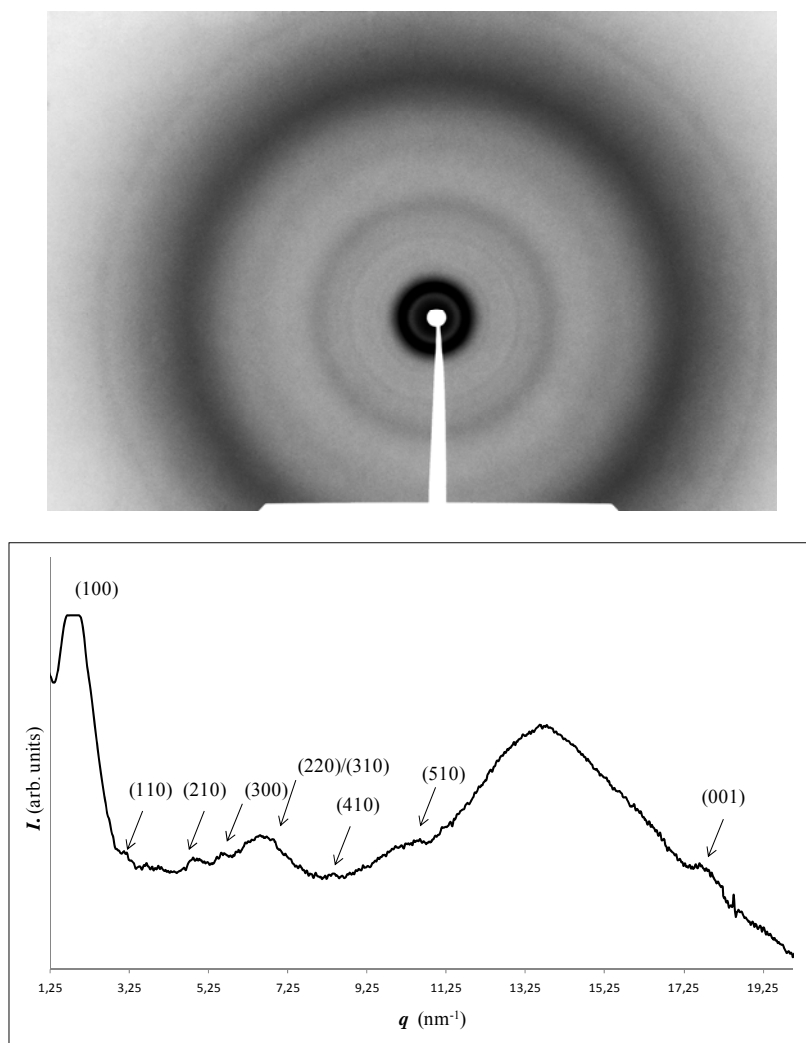


Figure S4. 2D diffraction pattern and 1D representation obtained from x-ray experiments carried out at room temperature in the crystal phase (eight weeks after thermal treatment).

A hexagonal columnar arrangement in the crystalline phase can be deduced by the presence of low-angle sharp maxima with a reciprocal spacing ratio $1:\sqrt{3}:\sqrt{7}:\sqrt{9}:\sqrt{12}:\sqrt{13}:\sqrt{21}:\sqrt{31}$. These maxima can be indexed as the (10), (11), (21), (30), (22)/(31), (41) and (51) reflections of a 2D hexagonal lattice with a lattice parameter $a = 39.3 \text{ \AA}$. In addition, though some liquid disorder is still visible at high angles, a sharp wide-angle maximum is observed, which can be attributed to a long-range stacking distance $h = 3.5 \text{ \AA}$. Furthermore, the relatively small intermolecular spacing along the column, 3.5 \AA , is in accordance to the unusual high-angle position of the diffuse reflection in the mesophase. Assuming the hexagonal arrangement, the resulting mass density of the structure is $\rho = M/(N_A a^2 h \sqrt{3}/2)$, where N_A is

the Avogadro number and M the molecular mass. Taking $M = 2372$ g/mole we get $\rho = 0.9$ g/cm³, which seems reasonable.

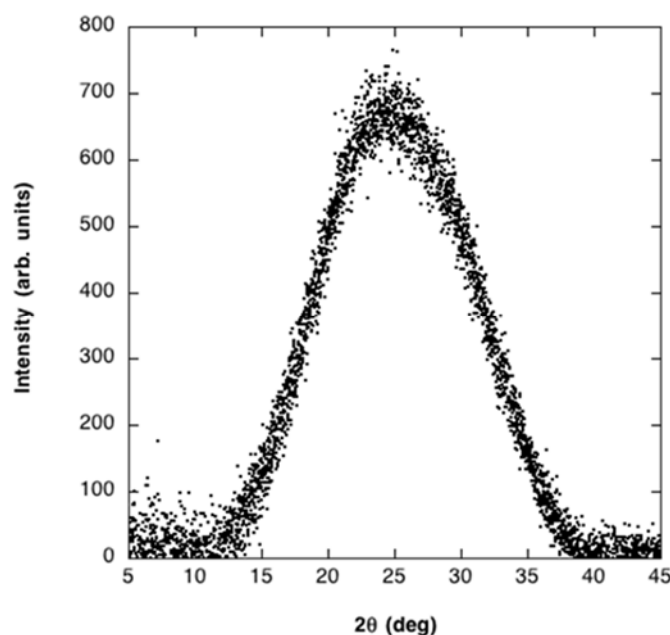


Figure S5. X-ray pattern of the mesophase in the wide-angle region. The diffuse halo covers an unusual broad region ranging from 6 Å ($2\theta = 14^\circ$) to 2.5 Å ($2\theta = 37^\circ$), with a maximum at 3.5 Å ($2\theta = 25^\circ$).

Table S1: X-ray diffraction data of the columnar mesophase and the crystal phase of **1**: proposed indexing, observed and calculated maximum and lattice constant.

Temp. (°C)	phase	hk	d_{obs} (Å)	d_{calc} (Å)	Hexagonal Lattice Parameter (Å)
r.t. ^a	Col _h	10	33.8	33.8	$a = 39.0$
r.t. ^b	Cr	10	34	34	$a = 39.3$
		11	19.8	19.6	
		21	13	12.9	
		30	11.2	11.3	
		22/31	9.6	9.8/9.4	
		41	7.5	7.4	
		51	5.9	6.1	
			4.6 ^c		
			3.5		

^a X-ray diffractogram recorded at room temperature after heating up to the isotropic liquid and cooling down the sample at a rate of ca. 10 °C/min. ^b X-ray diffractogram recorded at room temperature eight weeks after thermal treatment (heating up to the isotropic liquid and cooling down the sample at a rate of ca. 10 °C/min). ^c Diffuse maximum

SHG MEASUREMENTS

Analysis of the SHG and estimation of the degree of polar order in the Col phase of 1

To analyze the SHG results we recall that the nonlinear optical susceptibility tensor for the liquid crystal sample is given by

$$d = \begin{pmatrix} 0 & 0 & 0 & 0 & d_{15} & 0 \\ 0 & 0 & 0 & d_{15} & 0 & 0 \\ d_{31} & d_{31} & d_{33} & 0 & 0 & 0 \end{pmatrix} \quad (\text{S1})$$

where the field-induced optical axis (parallel to the hexagonal axis of the columnar structure) is the z axis. Since the material is absorbing at the SHG frequency (see Figure S6) the Kleinman symmetry ($d_{15} = d_{31}$) has not been assumed. The absorption coefficient at $\lambda/2=532$ nm is $\alpha=1.73 \mu\text{m}^{-1}$.

The effective susceptibility d_{eff} depends on the polarization of the incident and SHG beams. With reference to Fig. 3b of the main text, a σ polarized fundamental light produces a harmonic wave which is π polarized, with

$$d_{\text{eff}} = d_{31} \sin \theta', \quad (\text{S2})$$

where θ' is the angle of refraction inside the sample. On the other hand, if the fundamental light is π polarized, the SHG light results again to be π , with

$$d_{\text{eff}} = \left[(2d_{15} + d_{31}) \cos 2\theta' + d_{33} \sin 2\theta' \right] \sin \theta'. \quad (\text{S3})$$

As the absorption is only important for 2ω , the dependence of the SHG intensity I on the angle of incidence θ of the sample is given by^{iv}

$$I(\theta) = CI_0^2 l^2 d_{\text{eff}}^2 \exp(-\alpha l / 2) \frac{\left[\sinh^2(\alpha l / 4) + \sin^2(\Delta k L \cos \theta' / 2) \right]}{\left[(\alpha l / 4)^2 + (\Delta k L \cos \theta' / 2)^2 \right]}, \quad (\text{S4})$$

where C is a constant, I_0 the fundamental light intensity, $l=L/\cos\theta'$ the interaction length (L is the sample thickness), and $\Delta k=(2\pi/\lambda)\Delta n$, where Δn is the index mismatch between the fundamental and second harmonic lights.

The absorption data indicate $\alpha L=8.65 \gg 1$. Thus (S4) can be simplified for moderate angles of incidence to

$$I(\theta) = \frac{CI_0^2 d_{\text{eff}}^2}{\left[(\alpha / 4)^2 + (\Delta k / 2)^2 \right]}. \quad (\text{S5})$$

The experimental results for ($\sigma \sigma \rightarrow \pi$) conversion are in agreement with the shape of the curve $I(\theta)$ given by (S5) and (S2) (see Fig. 3c). By fitting these results and comparing them with the size of the SHG signal measured at the first Maker fringe of a y -cut quartz plate ($d_{11}=0.4$ pm/V), we deduced $d_{31}=0.5$ pm/V at 40 °C for a sample grown under an electric field of 12 V/ μm . For the fit we estimated $\Delta n = 0.08$, which is the dispersion parameter of a similar subphthalocyanine based material^v with analogous absorption characteristics. The results for the ($\pi \pi \rightarrow \pi$) conversion can also be fitted to (S5) and (S3) (the experimental curve is similar to that in Fig. 3b), but this fit does not allow to

separate the d_{31} , d_{15} and d_{33} coefficients with reasonable uncertainty, and will not be considered in the present work.

The degree of polar order is estimated from the analysis of the correlation between d_{ij} and the molecular hyperpolarizabilities β_{ij} . If a perfect molecular ordering is assumed (all dipole moments are parallel to the macroscopic polar axis) the maximum d_{31} coefficient achievable in the material, d_{31}^{\max} , would be

$$d_{31}^{\max} = Nf^3\beta_{31}, \quad (\text{S6})$$

where N is the density of molecules and f is a local field factor. These quantities are calculated to be $N = 2.5 \times 10^{20} \text{ cm}^{-3}$ (assuming that the material has a mass density of 1 g/cm^3) and $f^3 \approx 3$ (using the Lorentz expression for the local field factor and a refractive index $n=1.52$). Finally we have taken $\beta_{31}=9 \times 10^{-30} \text{ esu}$,^v which is the β_{31} coefficient of a similar trinitro subphthalocyanine molecule (there are no published results for **1**).

That molecule is supposed to have larger hyperpolarizabilities than **1**, because it has three surrounding strong acceptor substituents (NO_2) directly attached to the subphthalocyanine central core instead of the flexible peripheral elements of **1**. Thus the d_{31}^{\max} value calculated in this way must constitute an upper limit for the saturation value of d_{31} in C3. Using (S6) we obtain $d_{31}^{\max} = 0.35d_{31}$, where d_{31} is the actual value for a LC sample of **1** grown by cooling from the isotropic phase under $12 \text{ V}/\mu\text{m}$. This means that such a field induces a degree of polar order in the mesophase of at least 35%.

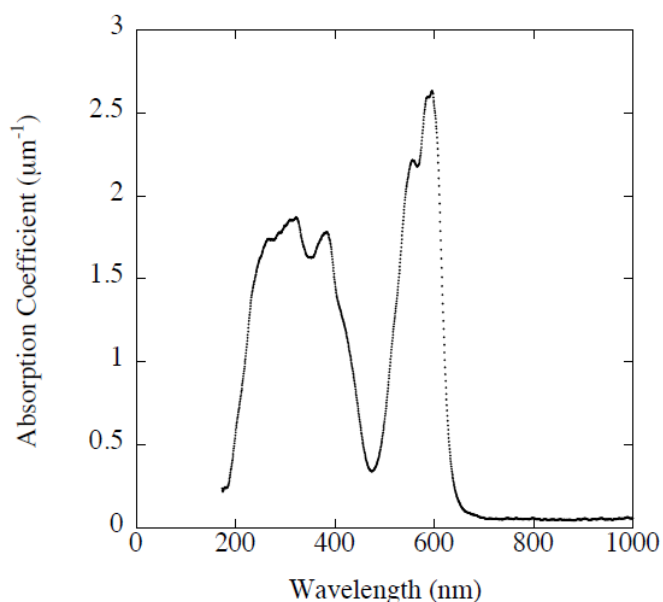


Figure S6. Absorption spectrum of **1** at room temperature.

THEORETICAL CALCULATIONS

All calculations were carried out by using the semiempirical PM7 method implemented in the MOPAC 2012 program.^{vi} The PM7 method has been parameterized to provide an accurate description of noncovalent molecular complexes.^{vii} The MOZYME technique was used in the optimization process to alleviate the computational cost. The optimization process was achieved with a gradient norm less than 50 kcal/mol Å and an energy difference less than 0.90 kcal/mol. Note that tighter criteria for the optimization process are difficult to be fulfilled due to the large size of the hexagonal columnar model (11564 atoms) and also to the flexibility of the peripheral alkyl chains. No constrain was imposed during the optimization process. Single-point calculations of columnar aggregates of increasing length were performed to study the evolution of the dipole moment with the size of the system. These columnar aggregates (tetramer, octamer, dodecamer, hexadecamer, and icosamer) were constructed using a columnar tetramer extracted from the PM7-optimized hexagonal structure as a building block. An intermolecular B···B distance of 4.32 Å was used. Single-point calculations under the influence of an external electric field (12 V/μm) were performed on the columnar icosamer. Figures S7 and S8 illustrate the structural characteristics and intermolecular interactions along a columnar aggregate and between vicinal columnar aggregates. Figure S9 shows the evolution of the dipole moment with the size of the columnar aggregate. In all of these Figures carbon atoms are shown in dark green, oxygen in red, nitrogen in blue, boron in weak pink, fluorine in pale green, and hydrogen in white.

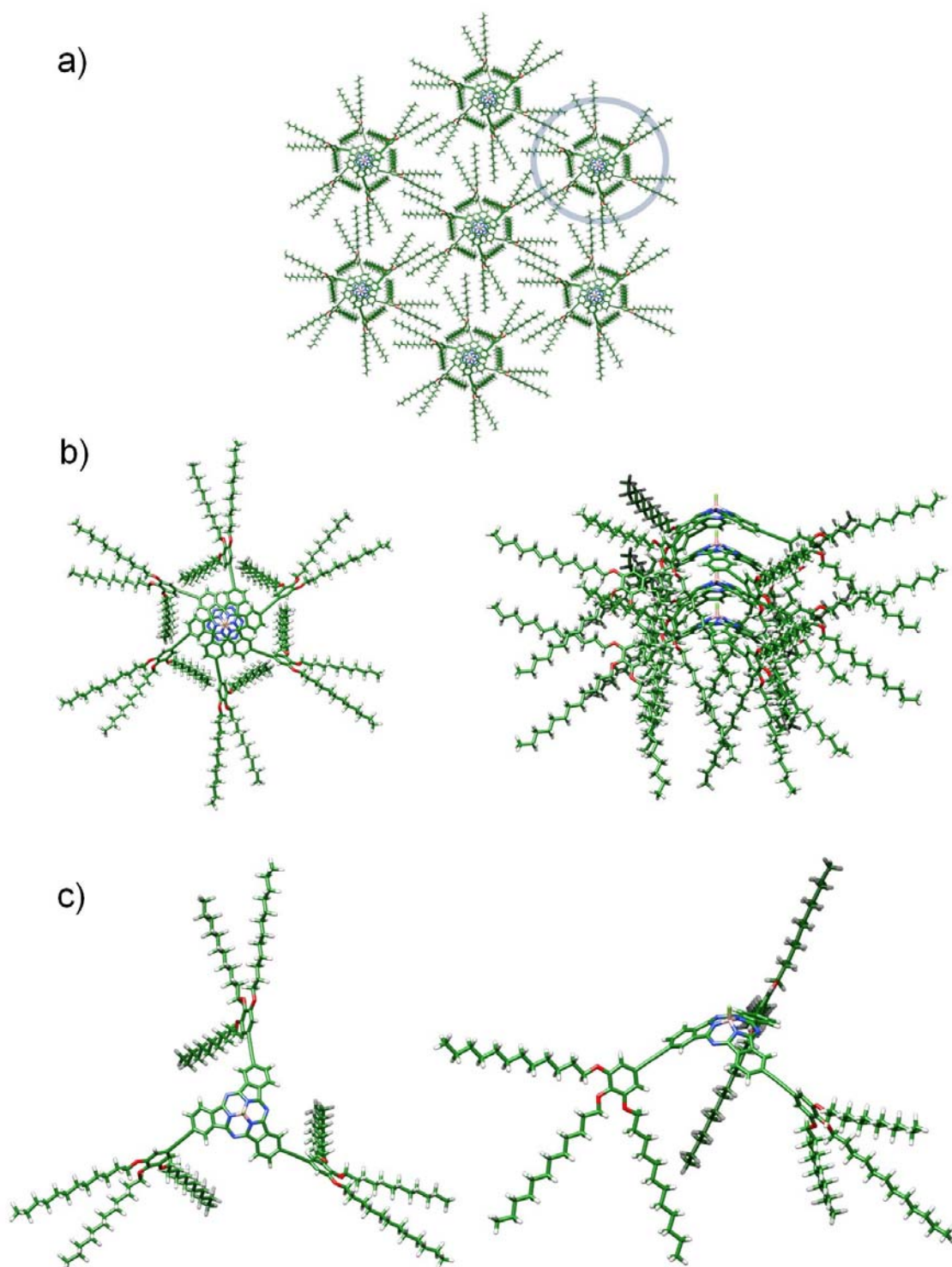


Figure S7. a) Top view of the PM7-optimized hexagonal columnar model for **1**. b) Top and side view of a columnar aggregate of the hexagonal columnar structure. c) Top and side view of **1** in the self-assembly.

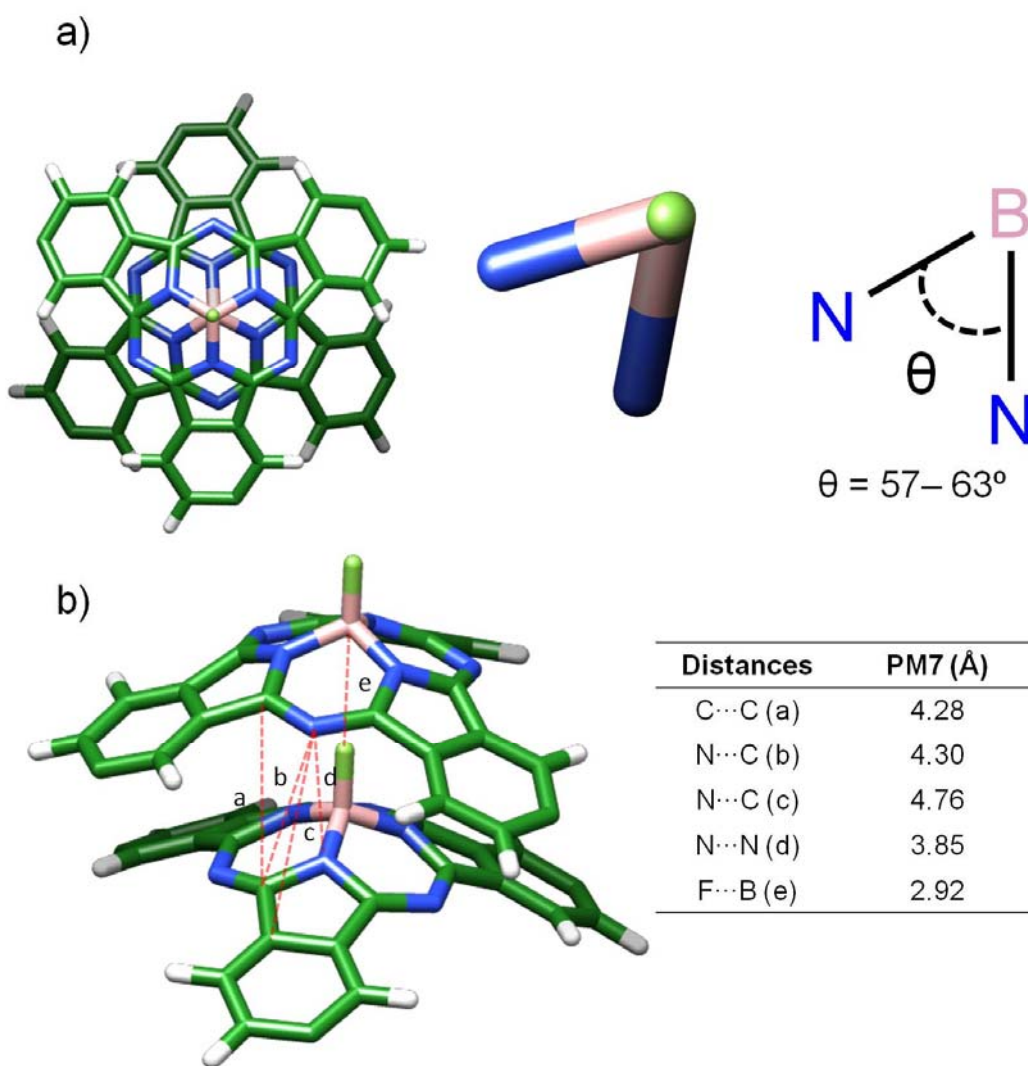


Figure S8. a) Top view of a simplified columnar dimer extracted from the PM7-optimized hexagonal structure where the terminal substituents have been deleted for simplicity. The range calculated for the twisting angle θ between adjacent SubPc cores is indicated. b) Side view of the dimer and values of the closest intermolecular contacts between the π -conjugated SubPc cores. Within a columnar arrangement, the $F^{\delta-} \cdots B^{\delta+}$ contacts between adjacent molecules are calculated at 2.92 Å, which is slightly longer than two times the covalent B–F bond (1.37 Å) and significantly shorter than the sum of the van der Waals radii of boron (1.92 Å) and fluorine (1.47 Å). This evidences the strong electrostatic interaction between B–F dipole units along the stacks.

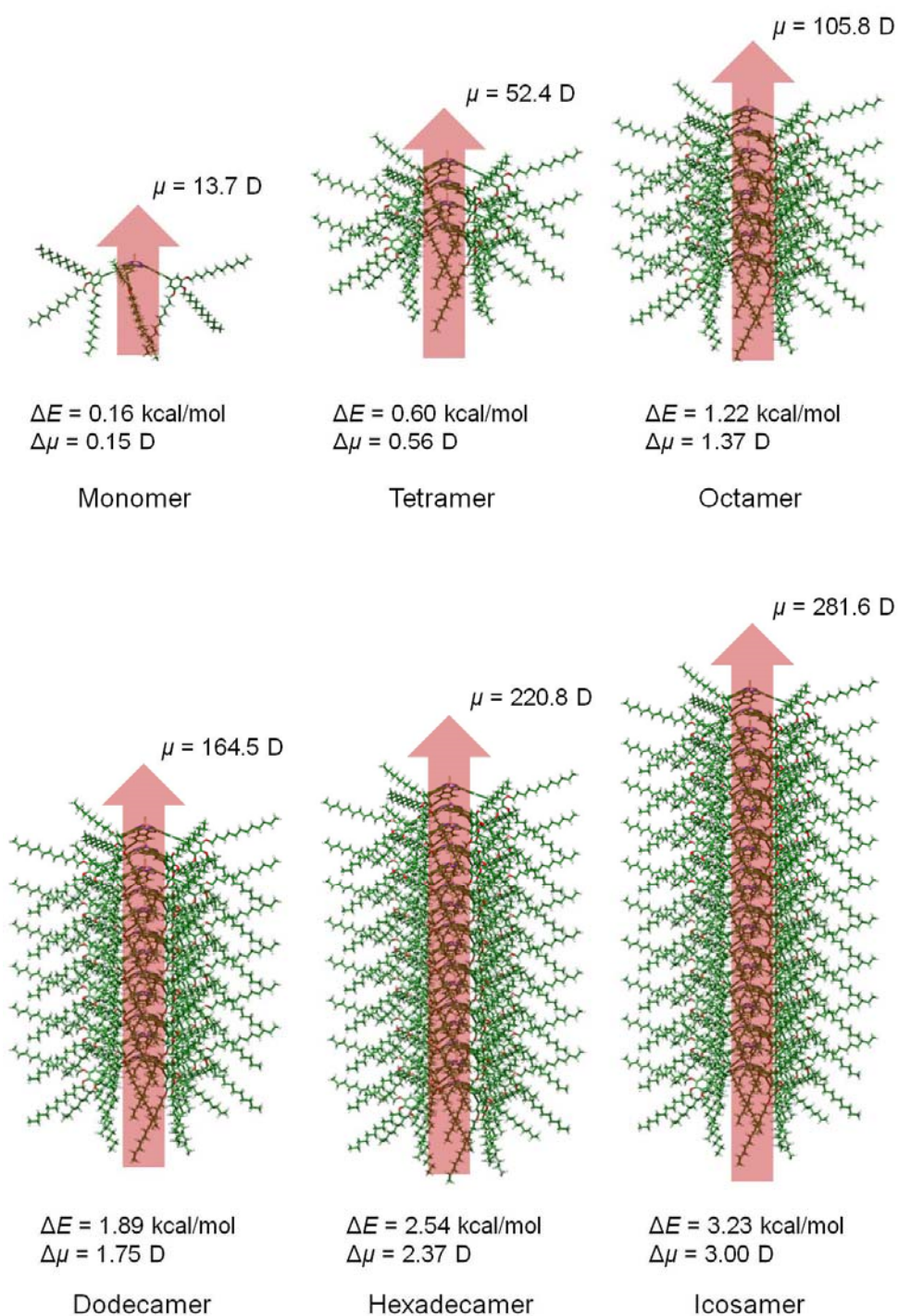


Figure S9. Direction and magnitude of the dipole moment (μ) computed for columnar aggregates of increasing length. An electric field of 12 V/ μm was then applied parallel and antiparallel to the dipole moment and the energy difference (ΔE) between both orientations was evaluated for each aggregate. ΔE increases linearly with the stack size (by about 0.15 kcal/mol per stacked molecule), reaching 3.2 kcal/mol in the icosamer. The presence of the electric field also leads to a slight increase/decrease in the dipole moment ($\Delta\mu$) when it is applied in the same/opposite direction, respectively, of the polarization vector of the columnar aggregate.

REFERENCES (S.I.)

- ⁱ J. Wu, M. D. Watson, L. Zhang, Z. Wang and K. Müllen, *J. Am. Chem. Soc.*, **2004**, *126*, 177–186.
- ⁱⁱ C. G. Claessens, M. J. Vicente-Arana, Tomás Torres, *Chem. Commun.*, **2008**, 6378–6380.
- ⁱⁱⁱ a) M. V. Fulford, D. Jaidka, A. S. Paton, G. E. Morse, E. R. L. Brisson, A. J. Lough, T. P. Bender, *J. Chem. Eng. Data*, **2012**, *57*, 2756–2765. b) M. S. Rodríguez-Morgade, C. G. Claessens, A. Medina, D. González-Rodríguez, E. Gutierrez-Puebla, A. Monge, I. Alkorta, J. Elguero, T. Torres, *Chem. Eur. J.* **2008**, *14*, 1342–1350.
- ^{iv} W. N. Herman, L. M. Hayden, *J. Opt. Soc. Am. B*, **1995**, *12*, 416.
- ^v G. Rojo, F. Agulló-López, B. del Rey, T. Torres, *J. Appl. Phys.* **1998**, *84*, 6507.
- ^{vi} J. J. P. Stewart, MOPAC, Stewart Computational Chemistry, Colorado Spring, CO., USA, 2012. <http://OpenMOPAC.net>.
- ^{vii} J. J. P. Stewart, *J. Mol. Model.*, **2013**, *19*, 1-32.